Contents lists available at ScienceDirect

Spectrochimica Acta Part A: Molecular and Biomolecular Spectroscopy

journal homepage: www.elsevier.com/locate/saa

Structural, vibrational and electronic spectroscopic study of 6-hydroxycoumarin using experimental and theoretical methods

D. Vijay [a], Y. Sushma Priya [b], M. Satyavani [a], Asim Kumar Das [c], B.N. Rajasekhar [c], A. Veeraiah [a,*]

[a] Molecular Spectroscopy Laboratory, Department of Physics, D.N.R. College (A), Bhimavaram 534202, India
[b] Department of Physics, Adikavi Nannaya University, Rajamahendravaram A.P-533296, India
[c] Atomic& Molecular Physics Division, BARC, Mumbai, India

ARTICLE INFO

Article history:
Received 10 April 2019
Received in revised form 4 December 2019
Accepted 6 December 2019
Available online 09 December 2019

Keywords:
6-Hydroxycoumarin (6HC)
TD-DFT
MESP
FT-IR
UV–Vis spectra

ABSTRACT

Understanding the photochemical behavior of structural isomers of hydroxycoumarin (HC) having different properties of consequence in biological activities demand spectroscopic information of this class of compounds. Barring 6-hydroxycoumarin (6-HC), other isomers of HC's are well studied spectroscopically. To understand and compare the photochemical activity of 6-HC with other isomers, a detailed study of this molecule has been taken up. For this purpose, electronic, vibrational and structural properties of 6-HC have been studied using ultraviolet absorption and Infrared spectroscopy techniques. Quantum chemical calculations have been performed at DFT/B3LYP level of theory to get the optimized geometry and vibrational frequencies of normal modes to support and analyze experimental data. The detailed vibrational assignments were made on the basis of potential energy distributions. Chemical activity, molecular orbital energies, band gap and hyper-polarizability information have been computed from quantum chemical simulations. NBO analysis helped in understanding the stability of the molecule arising from hyper-conjugative interaction and charge delocalization. UV–Visible spectrum of the compound was recorded in the region 300-600 nm helped in obtaining band gap data of the compound. Molecular Electrostatic Potentials (MESP) were plotted and the respective centers of electrophilic and nucleophilic attacks were predicted with the help of Fukui functions calculations. Further, it was observed that the negative electrostatic potential regions are mainly localized over the oxygen atoms and the positive regions are localized over the benzene ring. Details of the results and analysis of experimental and theoretical spectroscopy studies are presented in this paper.

© 2019 Elsevier B.V. All rights reserved.

1. Introduction

Coumarins, otherwise called as benzopyrones, because of their chemical activity can interact with enzymes over a wide range of biological activities such as anticoagulant, anticancer, antioxidant, antiviral, anti-diabetics, anti-inflammatory, antibacterial, anti-fungal and anti-neurodegenerative agents apart from fluorescent sensors [1]. Hydroxyl coumarins (HC) are found to be having biologically different importance [2] depending on the position of OH group substitution on the coumarin ring. For example 4-hydroxycoumarin is a carcinogen, 7-hydroxycoumarin has great significance as natural fragrances, whereas 6-hydroxycoumarin (6-HC) is found to be used as an anticancer agent [3–5]. 6-HC have number of applications in medical, dyes, cosmetics, food additive applications apart from solid state lightning applications [6–10]. Most of the organic synthesis use 6-hydroxycoumarin as key material as it is shows unique photochemical and photo physical properties [11,12]. Though a detailed spectroscopic information on other structural isomers of HC's is available in literature [13–17], surprisingly the spectroscopic data of 6-Hydroxycoumarin is very scarce. In this work, 6-HC has been studied experimentally using UV–Vis and Infrared techniques. Theoretical information obtained by simulations using density functional level of theory with hyper correlation function B3LYP at standard basis set 6-311++G (d, p)helped to consolidate structural geometry, vibrational frequencies, optical properties, HOMO-LUMO, NBO and Molecular Electrostatic Potentials (MESP). In this paper, UV–Vis and FT-IR data of 6-HC are reported for the first time. Details of the experimental and theoretical results and analysis of the results obtained are presented in this paper.

2. Computational details

In these, quantum chemical calculations using hybrid function Becke's parameter nonlocal hybrid exchange potential and the nonlocal correlation functional of Lee, Yang and Paar (B3LYP) with higher basis set 6-311++G(d, p) are performed using Gaussian09W package installed in PC series i3-4170 CPU @ 3.70 GHz processor system [18,19] and the optimized structure is visualized by GaussView 5.0.9

* Corresponding author.
E-mail address: avru@rediffmail.com (A. Veeraiah).

https://doi.org/10.1016/j.saa.2019.117930
1386-1425/© 2019 Elsevier B.V. All rights reserved.

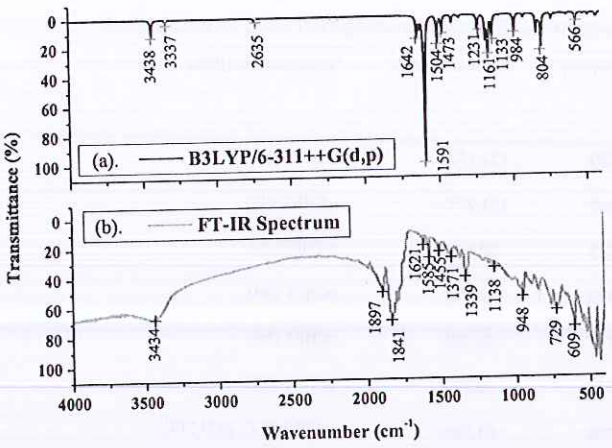

Fig. 3. Visualization of the molecular orbital of 6-hydroxycoumarin [HOMO–MO:42 and LUMO–MO:43].

over the and scan range 4000 cm^{-1} to 400 cm^{-1} with 64 number of scans at resolution 4 cm^{-1}.

4. Result and discussion

4.1. Molecular geometry

6-Hydroxycoumarin was optimized, the respective bond length, bond angles and dihedral angles were compared with experimental XRD data of a similar compound since the experimental XRD data of the titled compound hasn't been reported so far [24]. The molecular geometry of 6-HC was optimized using Gaussian09W, visualized by GaussView 5.0.9 and it is presented Fig. 1. Bond length, bond angles and dihedral angles of theoretical data along with experimental values were reported in Table 1. From Table 1, it can be observed that the aromatic ring C—C bond lengths and C-C-C bond angles are closer to the experimental bond lengths. Potential energy surface scan is the exact method to find transition states as it helps to find exact stationary points [25]. The PES was performed by changing dihedral angle C1-C6-O18-H15 from 0° to 360° with an interval of 10°. The potential energy curve shows broad peak at stable energy (E = −572.3963Hartrees) corresponding to a dihedral angle of 180°. The potential energy surface curve is presented in Fig. 2. Fig. 3, it shows the optimized geometry of molecule in equilibrium state.

4.2. Vibrational analysis

The titled compound 6-HC is considered under C_1 symmetry, contains 18 atoms. As a nonlinear molecule executes 3N-6 number of potentially observable active fundamental frequencies, 6-HC has 48 fundamental modes of vibrations. The internal coordinates as listed in Supplementary material 1 were used to define local symmetry coordinates. The local-symmetry coordinates were defined by following the recommendations of Pulay et al. [26,27], values of corresponding scale factors used to correct the B3LYP/6-311G++ (d, p) force field calculations are presented in Table 2. The in-plane and out-of-plane symmetry vibrations are found by the formula,

$$\Gamma 3N-6 = 35A'(\text{in-plane}) + 13A''(\text{out-of-plane}) \quad (1)$$

Table 2
Definition of local-symmetry coordinates and the values of corresponding scale factors used to correct the B3LYP/6-311G++ (d, p) force field calculations of 6-hydroxycoumarin.

No. (i)	Symbol[a]	Definition[b]	Scale factors
Stretching			
1–6	ν(C—C)(Ring1)	R1, R2, R3, R4, R5, R6	0.992
7–11	ν(C—C)(Ring2)	R7, R8, R9, R10, R11	0.702
12–13	ν(C—O)sub	R12, R13	0.778
14–16	ν(C—H)(Ring1)	R14, R15, R16	0.749
17–18	ν(C—H)(Ring2)	R17, R18	0.994
19	ν(O—H)(sub)	R19	0.800
In-plane bending			
20–21	βRtri	(γ 20 − γ 21 + γ22 − γ 23 + γ24 − γ25) / √6, (γ 26 − γ 27 + γ28 − γ 29 + γ30 − γ31) / √6	0.998, 0.958
22–23	βRasy	(2γ 20 − γ 21 − γ22 + 2γ23 − γ24 − γ25) / √12, (2γ 26 − γ 27 − γ28 + 2γ29 − γ30 − γ31) / √12	0.998, 0.958
24–25	βRsym	(γ 21 − γ22 + γ24 − γ25) / 2, (γ 27 − γ28 + γ30 − γ31) / 2	0.998, 0.958
26–30	β(C—H)	(γ32 − γ33) / √2, (γ34 − γ35) / √2, (γ36 − γ37) / √2, (γ 38 − γ39) / √2, (γ 40 − γ41) / √2	0.979
31	β(C—O)	(γ 42 − γ43) / √2	0.783
32	β(C-OH)	γ 44	0.948
33	β(C-C-O)	(γ 45 − γ46) / √2	0.995
Out of plane bending			
34–38	ω (C—H)	ρ47, ρ48, ρ49, ρ50, ρ51	0.950
39–40	ω (C—O)	ρ52, ρ53	0.912
Torsion			
41–42	τ RING tri	(τ 54 − τ55 + τ56 − τ57 + τ58 − τ59) / √6, (τ 60 − τ61 + τ62 − τ63 + τ64 − τ65) / √6	0.884,0.921
43–44	τ RING asy	(τ 54 − τ56 + τ57 − τ59) / 2, (τ 60 − τ62 + τ63 − τ65) / 2	0.884,0.921
45–46	τ RING sym	(−τ54 − 2τ55 − τ56 + τ57 + 2τ58 − τ59) √ 12, (−τ60 − 2τ61 − τ62 + τ63 + 2τ64 − τ65) √ 12	0.884,0.921
47	τ BUTT	(τ66 − τ67) / 2	0.992
48	τ CCOH	(τ68 − τ69) / 2	0.913

Where a = cos144°, b = cos72°.
Abbreviations: ν, stretching;β, in plane bending; ω, out of plane bending; τ, torsion, tri, trigonal deformation, sym, symmetrical deformation, asy, asymmetric deformation, butt, butterfly, sub, substitution.
[a] These symbols are used for description of the normal modes by PED.
[b] The internal coordinates used here are defined in the table given in Supplementary material 1.

Table 3 (*continued*)

Mode no.	FT-IR experimental frequencies (cm^{-1})	Theoretical frequencies (cm^{-1})		[b]IR intensity	[c]Raman activity	[d]Assignments (PED)
		[a]Scaled	Unscaled			
37	-	483	506	7.684	2.641	βCO (29)
38	-	431	454	10.405	0.331	τR1asy (42), τBUTT (28)
39	-	423	438	10.660	10.997	βCCO (25), βR2asy (23), βCO (18)
40	-	365	385	1.206	2.911	τR2asy (25), τR1asy (20), ωCH (17)
41	-	361	381	4.548	14.273	βCCO (22), υ CCR2 (20), βR1sym (19)
42	-	340	356	4.003	0.311	ωCH (27), τR2tri (21), τR2asy (17)
43	-	274	274	108.187	1.596	τCCOH (86)
44	-	243	255	1.773	0.346	υ CCR2 (22), βCCO (20), βR2sym (15)
45	-	172	180	0.657	0.153	τR2tri(30), τ R1sym (19), τ R2asy (16)
46	-	148	155	1.788	0.717	τR2sym (33), τBUTT (20)
47	-	75	78	1.741	0.149	τR2asy (32),τR2sym (24),τR2tri (21)
48						

Abbreviations: υ, stretching; β, in plane bending; ω, out of planebending; τ, torsion, ss, symmetrical stretching, as, asymmetrical stretching, sc, scissoring, wa, wagging, twi, twisting, ro, rocking, ipb, in-planebending, opb, out-of -planebending; tri, trigonal deformation, sym, symmetrical deformation, asy, asymmetric deformation, butter, butterfly, ar, aromatic, sub, substitution, vs, very strong; s, strong; ms, medium strong; w, weak; vw, very weak.

[a] Scaling factor: 0.74 above 3000 cm^{-1} and 0.743 below 3000 cm^{-1} for B3LYP/6-311++G(d,p).

[b] Relative absorption intensities normalized with highest peak absorption equal to 100.

[c] Relative Raman intensities normalized to 100.

[d] Only PED contributions ≥10% are listed.

The titled compound, 6-HC has C—C, C═O and O—H type of bonds. These bonds are involved in various stretching, bending and torsional vibrations. The calculated frequencies are scaled to achieve better match with the observed values. These vibrations along with the respective potential energy distribution percentages are tabulated in Table 3. The vibrational analysis of the respective modes is as follows.

4.2.1. C—C vibrations

In aromatic organic compounds, singlet and doublet of C—C ring vibrational frequencies are observed in the region 1400 cm^{-1}–1650 cm^{-1} [28]. In the present work, the scaled vibration at 1627 cm^{-1} was assigned to C—C stretching vibrations. This mode shows an excellent agreement with the observed value at 1621 cm^{-1}. C-C-C in plane and out-of-plane deformation is observed between 766 and 542 cm^{-1}. The scaled value at 731 cm^{-1} is assigned to C-C-C ring asymmetric deformation and the corresponding band is observed at 729 cm^{-1}. This is in synchronous with the scaled value.

4.2.2. Carbonyl functional group vibrations

Mostly, the dominant C═O in-plane stretching mode of vibration is located in the region 1600–1660 cm^{-1} [29]. In the present study, the band observed at 1585 cm^{-1} is assigned to C═O stretching vibration and the corresponding scaled value 1652 cm^{-1} shows a good agreement with the observed value as listed in the Table 3. Further, the C—O mode of vibrations is observed in the region 1000–1300 cm^{-1}. According to scaled quantum mechanical (SQM) force field calculation, we found C—O modes of vibrations around 1094 and 1285 cm^{-1}. COH in-plane bending is observed at 1198 cm^{-1} and its scaled value is 1161 cm^{-1}.

4.2.3. O—H vibrations

In general, the O—H functional group vibrations are present in the region 2500–4000 cm^{-1} [30]. The experimental FT-IR spectra of 6-HC compound having O—H vibrations around 3434 $cm^{-1}$and corresponding theoretical peak was observed around 3438 cm^{-1} as reported in Table 3.

4.3. NBO (natural bond orbital) analysis

Natural bond orbital analysis is used for molecular atomic charge and orbital population [31,32]. Most of NBO analysis is reported up to second order interactions. In the present work, the NBO calculations were performed on optimized structure of 6HC using NBO 6.0 which is embedded Gaussian09W program package. Here we observed second order perturbations and most of the bond interactions are occurring at lower population. Lone pair (LP) electrons are observed for O16, O17 and O18. The second order perturbations were studied to predict the donor-acceptor interaction in the natural bond orbital [33].

$$E^{(2)} = -n_\sigma \frac{\langle \sigma | F | \sigma \rangle^2}{\varepsilon_{\sigma^*} - \varepsilon_\sigma} = -n_\sigma \frac{F_{ij}^{\ 2}}{\Delta E} \quad (2)$$

The interactions of donor (i) -acceptor (j) were observed and the respective interactions of the titled compound were tabulated in Table 4. From the table, largest stabilization energy is observed for C9-C11 (π) – C12-O17 (π*) at 20.97 kJ/mol and lowest stabilization is occurred at 0.69 kJ/mol for C2-C3 (σ) – C3-O16 (σ*).

4.4. Frontier molecular orbitals

Highest occupied molecular orbital (HOMO) and lowest unoccupied molecular orbital (LUMO) study is related to the ionization potential and chemical reactivity of the molecule [34]. The total energy, HOMO, LUMO, difference between HOMO and LUMO, Ionization potential (I), Electron Affinity (A), Chemical potential (μ), Electronegativity (χ), Chemical hardness(η), Electrofilicity index (ω), Global Softness (σ), Total energy change(ΔE_T), Dipole moment(D) for the investigated compound 6HC is studied by DFT method with higher basis set B3LYP/6-311++G(d,p) basis set and the values are tabulated in Table 5. From the

Table 6
The electric dipole moment (D), average polarizability, first hyperpolarizability, etc., of 6-HC by quantum calculation.

μ and α components	B3LYP/6-311++G**	β components	B3LYP/6-311++G**
μ_x	1.6626	β_{xxx}	−344.4361
μ_y	1.4450	β_{xxy}	112.4676
μ_z	0.0009	β_{xyy}	−51.3494
μ(D)	4.8524	β_{yyy}	49.4611
α_{xx}	181.9068	β_{xxz}	0.0444
α_{xy}	−4.2111	β_{xyz}	0.0114
α_{yy}	115.3935	β_{yyz}	−0.0245
α_{xz}	0.0015	β_{xzz}	22.7462
α_{yz}	0.0026	β_{yzz}	14.9624
α_{zz}	58.3966	β_{zzz}	−0.0133
Δα	$47.72213318 \times 10^{-24}$ esu		
α_o(esu)	17.57119×10^{-24}	βtotal (esu)	3.566699×10^{-30}

$$Softness(s) = \frac{1}{\eta} \tag{7}$$

4.5. UV–Vis spectrum

UV–Vis spectrums are recorded in the region 300–600 nm at Photophysics beamlineIndus-1, Indus-1, a 450 MeV synchrotron radiation source. Calibration of absorbance spectrum is presented with the help of α-coefficient formula given in Eq. (2). The resultant spectrum is shown in Fig. 5. From UV-Vis spectrum, where UV light start absorption from 334 nm and there is a strong absorption peak observed at 374 nm. Predicted TD-DFT spectra were given same absorption. In addition to that the calculated direct energy band gap was found at 3.9 eV. ($\propto = \ln\frac{I}{I_0}h\nu$).

4.6. NLO properties

Theoretical non liner optical (NLO) calculations gives information about the molecular electronic dipole moment (μ), the polarizability (α), and the first hyperpolarizability (β) which are difficult to calculate directly. Therefore, these three properties of the titled compound 6HC are calculated by using DFT method with higher basis set B3LYP/6-311++G(d, p) for the first time [35]. Polarizability and first order hyperpolarizability of the investigated compound using X, Y, Z elements can be calculated by using the following relations

$$\mu = \mu^2{}_x + \mu^2{}_y + \mu^2{}_z \tag{8}$$

$$\alpha_o = \frac{\alpha_{xx} + \alpha_{yy} + \alpha_{zz}}{3} \tag{9}$$

$$\Delta\alpha = 2^{-1/2}\left[(\alpha_{xx} - \alpha_{yy})^2 + (\alpha_{yy} - \alpha_{xx})^2 + 6\alpha^2{}_{xx}\right]^{1/2} \tag{10}$$

$$\beta = \left(\beta^2{}_x + \beta^2{}_y + \beta^2{}_z\right)^{1/2} \tag{11}$$

and

$$\beta_x = \beta_{xxx} + \beta_{xyy} + \beta_{xzz} \tag{12}$$

$$\beta_y = \beta_{yyy} + \beta_{xxy} + \beta_{yzz} \tag{13}$$

$$\beta_z = \beta_{zzz} + \beta_{xxz} + \beta_{yyz} \tag{14}$$

The calculated values which are in atomic units (a.u.) of the compound under investigation can be converted into electrostatic units (esu) and tabulated in Table 6. From the table calculated values of electronic dipole moment μ(D) is found to be 4.85246587, average polarizability (α): 1a.u = $47.72213318 \times 10^{-24}$ esu, first hyperpolarizability (β): 1 a.u = 3.566699×10^{-30} esu.

4.7. Molecular electrostatic potential (MESP)

Molecular electrostatic potential is used to determine the intermolecular interactions, nucleophilic and electrophilic attacks of the titled compound 6HC [36]. Most of recent studies on MESP analysis reported electronic distributions of molecule and visualizing electrophilic and nucleophilic attacks [37]. The calculated 3D electrostatic potential contour map is shown in Fig. 6. The figure shows that oxygen atoms are negatively charged and that is localized at red region. Positive charge localized at benzene ring is shown as blue region.

4.8. Mullikan atomic charge population analysis

Mulliken atomic charge population is extracted from the optimized Gaussian output file. The titled compound has 18 atoms and their corresponding Mulliken charges along with ATP charges are tabulate in Table 7. From atomic charge population, oxygen atoms O16, O17 and

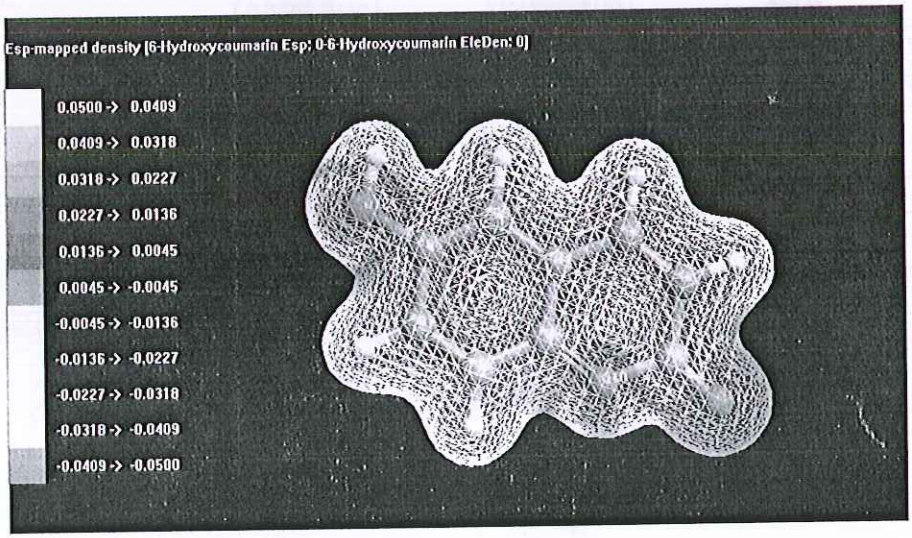

Fig. 6. B3LYP/6-311++G(d,p) calculated 3D molecular electrostatic potential maps of 6-hydroxycoumarin.

[14] Joanna TrykowskaKonc, Elżbieta Hejchman, Hanna Kruszewska, Irena Wolska, Dorota Maciejewska, European Journal of Medicinal Chemistry 46 (2011) 2252–2263.
[15] Joanna Trykowska Konc, Elżbieta Hejchman, Hanna Kruszewska, Irena Wolska, Dorota Maciejewska, Journal of Molecular Structure 930 (2009) 195–200.
[16] Sarvesh Kumar, Brajendra K. Singh, Neerja Kalra, Vineet Kumar, Ajit Kumar, Ashok K. Prasad, Hanumantharao G. Raj, Virinder S. Parmar, Balaram Ghosh, Bioorganic & Medicinal Chemistry 13 (2005) 1605–1613.
[17] Kinga Ostrowska, Elżbieta Hejchman, Dorota Maciejewska, Agata Włodarczyk, Kamil Wojnicki, Dariusz Matosiuk, Agnieszka Czajkowska, Izabela Młynarczuk-Biały, Łukasz Dobrzycki, MonatsheftefürChemie - Chemical Monthly 146 (2015) 89–98.
[18] C. Lee, W. Yang, R.G. Parr, Phys. Rev. B 37 (1988) 785.
[19] M.J. Frisch, G.W. Trucks, H.B. Schlegel, G.E. Scuseria, M.A. Robb, J.R. Cheeseman, G. Scalmani, V. Barone, B. Mennucci, G.A. Petersson, H. Nakatsuji, M. Caricato, X. Li, H.P. Hratchian, A.F. Izmaylov, J. Bloino, G. Zheng, J.L. Sonnenberg, M. Hada, M. Ehara, K. Toyota, R. Fukuda, J. Hasegawa, M. Ishida, T. Nakajima, Y. Honda, O. Kitao, H. Nakai, T. Vreven, J.A. Montgomery Jr., J.E. Peralta, F. Ogliaro, M. Bearpark, J.J. Heyd, E. Brothers, K.N. Kudin, V.N. Staroverov, R. Kobayashi, J. Normand, K. Raghavachari, A. Rendell, J.C. Burant, S.S. Iyengar, J. Tomasi, M. Cossi, N. Rega, J.M. Millam, M. Klene, J.E. Knox, J.B. Cross, V. Bakken, C. Adamo, J. Jaramillo, R. Gomperts, R.E. Stratmann, O. Yazyev, A.J. Austin, R. Cammi, C. Pomelli, J.W. Ochterski, R.L. Martin, K. Morokuma, V.G. Zakrzewski, G.A. Voth, P. Salvador, J.J. Dannenberg, S. Dapprich, A.D. Daniels, O. Farkas, J.B. Foresman, J.V. Ortiz, J. Cioslowski, D.J. Fox, Gaussian 09, Revision A.1, Gaussian Inc, Wallingford, CT, 2009.
[20] R. Dennington, T. Keith, J. Millam, K. Eppinnett, W.L. Hovell, R. Gilliland, Gauss View, Version 3.09, Semichem, Inc., Shawnee Mission, KS, 2003.
[21] P. Pulay, G. Fogarasi, F. Pang, J.E. Boggs, J. Am. Chem. Soc. 101 (1979) 2550.
[22] Sundius, J. Mol. Struct. 218 (1990) 321.
[23] T. Sundius, Vibr. Spectrosc. 29 (2002) 89.
[24] H.M. Han, C.R. Lu, Y. Zhang, D.C. Zhang, ActaCryst. E 61 (2005) 1864.
[25] Scanning potential energy surface using gaussian, http://sf.anu.edu.au/~vvv900/gaussian/ts/scanning-pes.html.
[26] P. Pulay, J. Mol.Struct. 347 (1995) 293.
[27] G. Fogarasi, X. Zhou, P.W. Taylor, P. Pulay, J. Am. Chem. Soc. 114 (1992).
[28] M.V.S. Prasad, N. Udaya Sri, A. Veeraiah, V. Veeraiah, K. Chaitanya, J.At. Mol. Sci. 4 (2012) 1–17.
[29] G. Keresztury, S. Holly, J. Varga, G. Besenyei, A.Y. Wang, J.R. Durig, Spectrochimica. Acta A. 49 (1993) 2007.
[30] K.S. Smimov, et al., Vibrational Spectroscopy 4 (1993) 255–259.
[31] A.E. Reed, F. Weinhold, Natural localized molecular orbitals, J. Chem. Phys. 83 (1985) 1736–1740.
[32] Mehmet Karabacak, Leena Sinha, Onkar Prasad, Abdullah M. Asiri, Mehmet Cinar, Vikas K. Shukla, SpectrochimicaActa Part A: Molecular and Biomolecular Spectroscopy 123 (2014) 352–362.
[33] NBO 6.0 Program Manual, Natural Bond Orbital Analysis Programs compiled and edited by Frank Weinhold and Eric D. Glendening, A-27.
[34] Tahar Abbaz, Amel Bendjeddou, Didier Villemin, Pharmaceutical and Biological Evaluations 5 (2018) 27–39.
[35] J.N. Liu, Z.R. Chen, S.F. Yuan, J. Zhejiang Univ. B6 (2005) 584–589.
[36] Majid Ali, Asim Mansha, Sadia Asim, Muhammad Zahid, Muhammad Usman, Narmeen Ali, Journal of Spectroscopy 15 (2018).
[37] Yi Li, Yuanyuan Liu, Haowei Wang, Xiaohui Xiong, Ping Wei, Fangshi Li, Molecules 18 (2013) 877–893.